A R C H I V E S O F M E T A L L U R G Y A N D M A T E R I A L S
Volume 53 2008 Issue 2

M. KIRSCHEN*, C. RAHM*, J. JEITLER*, G. HACKL

STEEL FLOW CHARACTERISTICS IN CFD IMPROVED EAF BOTTOM TAPPING SYSTEMS

CHARAKTERYSTYKA PRZEPŁYWU STALI PRZY UŻYCIU CFD DO POPRAWY DOLNEGO SPUSTU Z EAF

The steel flow characteristics in electric arc furnace (EAF) bottom tapping systems were investigated using computational fluid dynamics (CFD) simulations for a large variety of tap channel geometries and four different EAFs. The results clearly demonstrated the advantages of a new conical tap channel design compared to the conventional cylindrical geometries, since for the same tap diameter the resulting mass flow rate was increased providing shorter tap-to-tap times. In addition, backflow with negative pressure patterns in the channel entry area was completely avoided with the conical design. Consequently, the steel flow turbulence intensity was significantly decreased resulting in a more stable steel jet during tapping. The maximum steel velocity and velocity gradients at the channel entry and the pressure differences at the channel walls were significantly decreased indicating a lower tendency for wear at the channel entry area and, therefore, an increased lifetime.

Typically, approaches to increase productivity and decrease tap-to-tap times have increased the tap diameter. However, the CFD simulations demonstrated that increasing the tap diameter resulted in earlier slag entrainment and an increased steel mass remaining in the EAF. Thereby, the yield was decreased for large tap diameters, although the tapping time may be decreased due to the higher mass flux. However, due to the desired late slag entrainment at maximum mass flux, selection of an appropriate conical tapping system maximizes tapping efficiency.

Keywords: Electric arc furnace, bottom tapping systems, computational fluid dynamics simulation

Charakterystyki przepływu stali w systemach z dolnym spustem w piecach łukowych były badane z użyciem symulacji obliczeniowej dynamiki płynów (CFD) dla dużej różnorodności geometrii otworów spustowych i czterech różnych pieców EAF. Wyniki wyraźnie wykazują zalety nowych stożkowych otworów spustowych w porównaniu do tradycyjnych cylindrycznych. Dla tej samej średnicy otworu spustowego został uzyskany większy przepływ masy, przy krótszym czasie od spustu do spustu. Ponadto, dzięki stożkowej geometrii otworu zostało całkowicie wyeliminowane cofanie stali przy podciśnieniu w strefie wlotu. W konsekwencji intensywność turbulencji przepływu stali znacząco się zmniejszyła, doprowadzając do bardziej stabilnego spustu stali. Maksymalna prędkość przepływu stali i gradient prędkości przy wlocie otworu oraz różnice ciśnień zostały znacznie zmniejszone, wykazując niższą tendencję zużywania się otworu spustowego, tym samym zwiększając jego żywotność.

Dotychczas zwiększanie wydajności i skrócenie czas wytopu realizowano poprzez zwiększanie średnicy otworu spustowego. Jednakże symulacje CFD wskazują, że zwiększenie średnicy skutkuje wcześniejszym zaciąganiem żużla i zwiększeniem masy stali pozostałej w piecu. Tym samym wydajność zmniejsza się przy dużych średnicach otworu, chociaż czas spustu jest krótszy przy większym przepływie masy.

1. Introduction

Bottom tapping systems are widely adopted in electric arc furnaces (EAFs) because they enable the amount of slag carryover to the ladle during tapping to be minimized. In addition, nitrogen pick-up is decreased and tapping is more rapid with the low furnace tilting angle and the tapping conditions are more constant. Slag-free tapping is possible when slag detection systems are used or with a liquid heel retaining tapping strategy. Maintenance requirements are reduced due to integrated automatic closure systems and the low risk of steel solidification in the tap channel. Whilst some older furnaces are equipped with spouts or runners, most of the new EAFs are equipped with bottom tapping systems, providing the advantage that the volume of refractory material is decreased as a runner or spout is not required.

The lifetime of tapping systems is usually in the order of a few hundreds heats. Semi-automatic tap changing systems (e.g., i-TAP® and the ETP-machine [1,2])

* RHI AG, TECHNOLOGY CENTER LEOBEN, MAGNESITSTR. 2, A-8700 LEOBEN, AUSTRIA
* RHI AG, MARKETING STEEL DIVISION, WIENERBERGSTR. 11, A-1100 VIENNA, AUSTRIA

enable hot tapping system changes with minimum furnace shutdown time and minimum maintenance requirements. The main wear mechanisms are hot erosion in the hearth area near the bottom tap, the tap inlet, and the tap outlet area due to high steel velocity at near-wall areas during tapping, in addition to possible oxidation of the end brick by air, and corrosion by slag. Increased taphole wear causes an increased mass flow rate with lifetime and subsequent adaptation of the tapping parameters. In order to improve the performance of bottom tapping systems, a new conical tapping system design has been introduced. In this paper the results from computational fluid dynamics (CFD) simulations of the steel flow in bottom tapping systems are presented to illustrate and highlight the influence of tap geometry on steel flow characteristics.

2. CFD simulations of steel flow in bottom tapping systems

Simulations were performed on bottom tapping systems used in a variety of customer EAFs with tapping weights ranging from 80 t to 250 t. In this paper a summary of the CFD simulation results from four EAFs (Table 1) are presented.

TABLE 1
Operating parameters of the four EAFs used in the described simulations

	EAF no. 1	EAF no. 2	EAF no. 3	EAF no. 4
Furnace type	DC	AC	AC	AC
Tapping weight [t]	170	85	80	250
Bottom tapping	EBT	EBT	EBT	EBT
Tap channel length [mm]	1230	950	1180	1200
Sill level above tap inlet * [mm]	730	350	530	600
Ferrostatic pressure at exit ** [105 Pa]	1.30	0.88	1.19	1.23

*: at 10 ° tilt angle, **: from nominal melt level

The initial steel bath sill level was determined from the nominal 100% furnace charging level. A 10° furnace tilt angle and a slag layer width of 150 mm were assumed.

The three-dimensional steel flow patterns in the tapping area were calculated using the Fluent 6.3 CFD software package. A section of the total furnace steel volume around the bottom tapping area was discretized into approximately 700,000 cells. Transient simulations of the steel flow were performed including a first-order implicit formulation and a Volume-of-Fluid (VOF) multiphase simulation comprising steel, slag, and gas phases. The turbulent viscous flow was modelled with a realizable k-ε model and the standard wall function used had a 1 mm roughness. The densities and viscosities of liquid steel and slag were set at 7000 kg/m^3, 0.005 kg/ms, 3000 kg/m^3, and 0.10 kg/ms, respectively.

3. Results

Having calculated the steel flow patterns, the focus was on: (1) the influence of the conical and cylindrical tap design and tap diameter on the velocity distribution, (2) the maximum mass flow rate at the beginning of tapping, (3) the turbulence distribution of the steel flow, (4) the pressure distribution in the tap channel, and (5) slag entrainment at the end of tapping.

3.1. Steel flow characteristics

The calculated velocity distributions in vertical cross section through a conical and cylindrical tap channel are shown in Figure 1 (170 mm tap diameter) and Figure 2 (190 mm tap diameter).

For the cylindrical design, the sharp edged inlet caused separation of the fluid from the tap channel wall near the inlet. When a second gas phase was not able to enter the channel (as assumed for these simulations) the fluid separation region was filled by steel in a recirculation zone with an upward-directed velocity component. However, real steel flow separation from the wall and filling of the recirculation zone by a gas phase is considered more likely. The potential gas phase consists of remaining air from the filling sand, precipitating CO gas from the saturated liquid steel at low pressure, or both. In all cases, the effective diameter of the tap channel was decreased for the cylindrical design. The mass continuity along the tap channel requires acceleration of the steel flow at the channel centre. However, by using the conical inlet design, the steel liquid separation zone was completely avoided. Due to turbulence dissipation at the separation region in the cylindrical geometry design, the steel flow pressure drop was higher than for the conical geometries (approximately 10% for turbulent flow and 50% for laminar flow). As a consequence, the resulting steel mass flow was lower for cylindrical geometries when compared to the conical design with the same diameter and ferrostatic pressure at the channel exit.

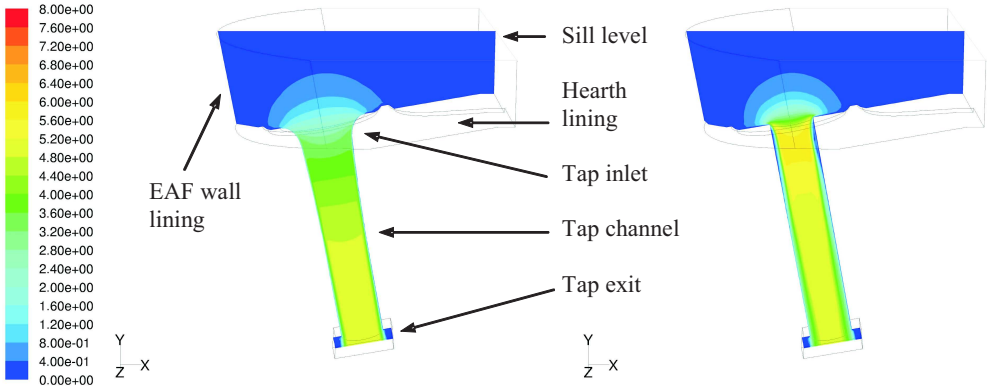

Fig. 1. Calculated steel velocity (m/s) in vertical cross section through the tap area, left: conical geometry, right: conventional cylindrical geometry (EAF no. 2, 170 mm tap diameter)

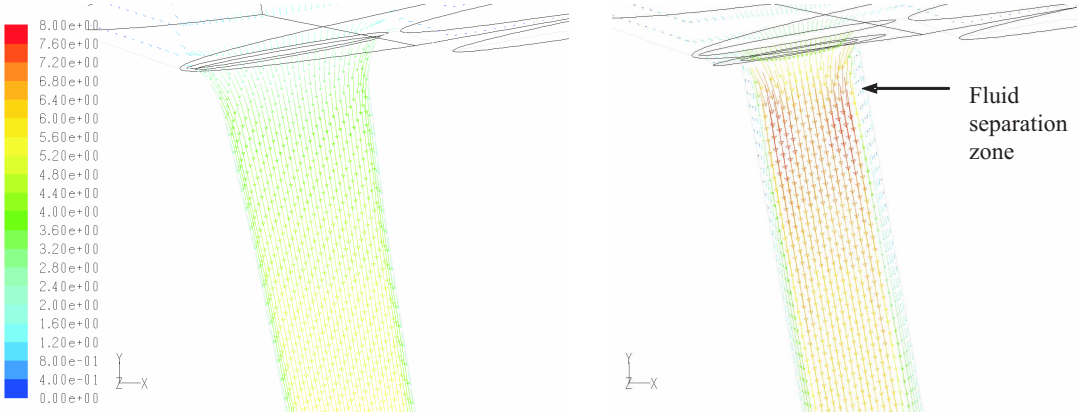

Fig. 2. Calculated steel velocity vectors (m/s) in vertical cross section through the tap area, left: conical geometry, right: conventional cylindrical geometry (EAF no. 1, 190 mm tap diameter)

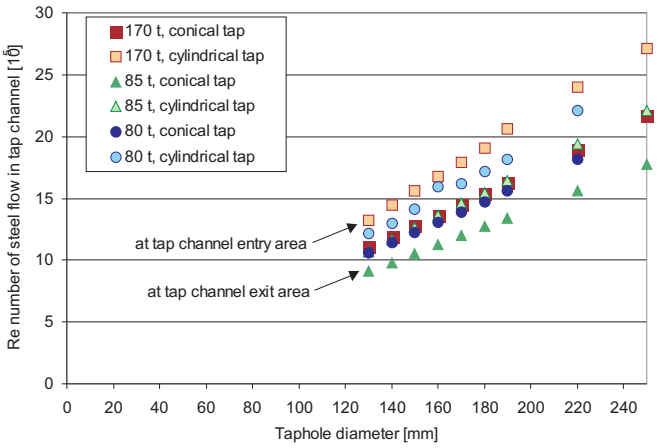

Fig. 3. Calculated maximum steel velocities and corresponding Re numbers increased with tap diameter for a given sill level above the tap exit

The maximum Re numbers of the steel flow are detailed in Fig. 3, indicating higher turbulences in the cylindrical design. For any given tap diameter, the maximum steel velocities in the channel inlet of the cylindrical design were higher than in the conical geometries (Figs. 1–2). The mean steel velocities increased slightly with tap diameter indicating a higher potential for erosion of the tap channel refractory.

From the velocity distribution, the mass flow rates for the simulated geometries were determined. Although the mass flow rate was calculated for a 10° tilt angle, it was assumed that the sill level remained comparable due to the furnace tilting. The calculated steel flow rates depended on the steel sill level above the tap exit, the geometry of the bottom tapping area, and the tapping angle (Fig. 4). By increasing the tap diameter to 250 mm, the maximum mass flow rate into the ladle approached 2 t/s.

The region of fluid separation from the channel wall with the cylindrical geometries generated steel flow turbulence near the channel wall (Fig. 5). Both the intensity and volume of the high turbulent flow region were higher for the cylindrical geometries. At the tap channel exit of the cylindrical design, the high turbulent flow region covered approximately half of the tap diameter (Fig. 6). This increased the mass transfer in the near-wall region and, therefore, erosion potential of the steel flow at the entire tap wall.

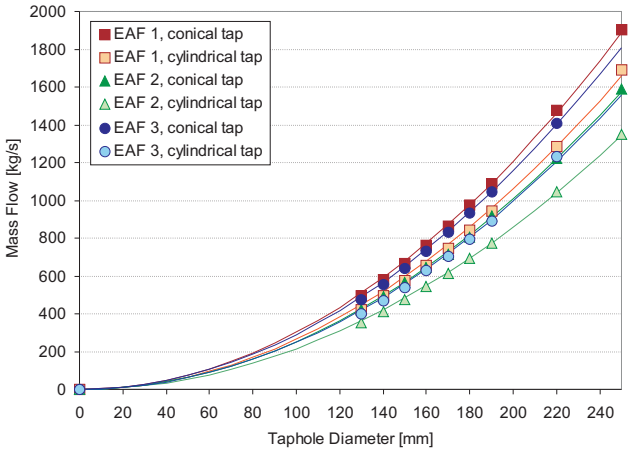

Fig. 4. Calculated maximum mass flow rates increased with tap diameter for a given sill level above the tap exit

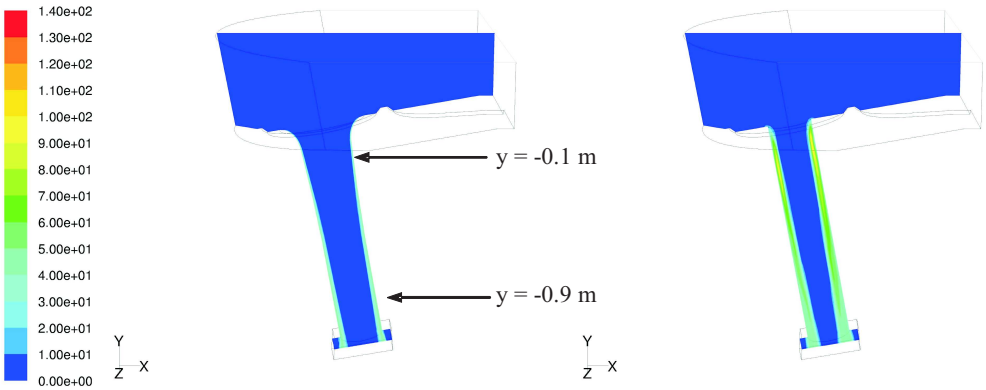

Fig. 5. Calculated relative turbulence intensities (%) in vertical cross section through the tap area, left: conical geometry, right: conventional cylindrical geometry (EAF no. 2, 170 mm tap diameter).

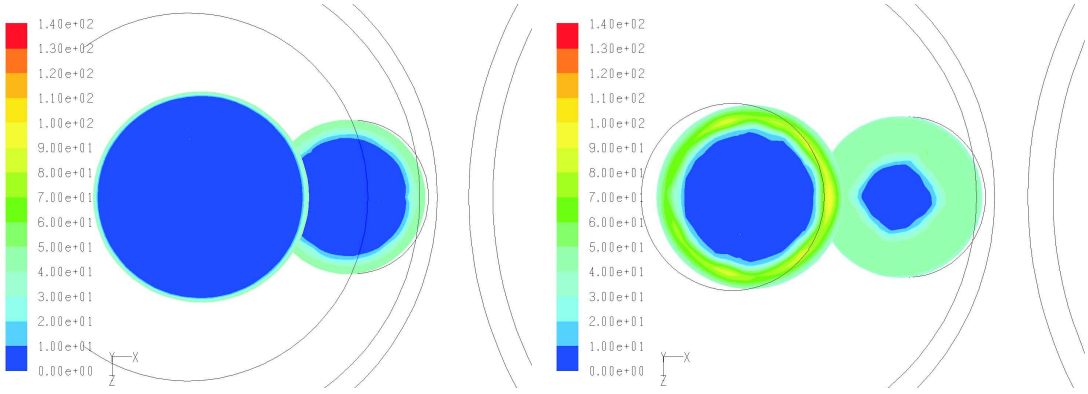

Fig. 6. Calculated relative turbulence intensities (%) at 0.1 m and 0.9 m below the tap inlet (horizontal cross sections), left: conical geometry, right: conventional cylindrical geometry (EAF no. 2, 170 mm tap diameter)

Typically, the characteristic length of an inlet duct flow region is 30–100 times the inlet diameter, namely significantly longer than the total EAF tap channel lengths. This meant that fluid separation in the cylindrical design influenced significantly the steel flow regime at the channel exit, and therefore the free steel stream into the ladle. For all simulated tap diameters, the mean turbulence of the steel flow in conical tap geometries was 30–45% lower than for cylindrical tap geometries (Fig. 7).

The fluid separation zone was characterized by low static pressure (Fig. 8). Operational experience and phase equilibrium calculations have shown that the typical steel melt composition at tapping with 0.1 wt.% carbon and 600 ppm oxygen is saturated with CO gas. In EAFs with purging systems the CO concentration is slightly lower. Therefore, at regions in the tap channel with pressures < 1 bar CO gas precipitates easily from the steel melt. It is most likely that the separation zone is filled with degassed CO gas from the steel melt, entrapped air, or both. Since neither CO degassing of the steel melt was considered in the simulations nor air entrapment in the VOF multiphase model, the calculated pressures were unrepresentatively low in the region of fluid separation in the cylindrical geometries. However, low-pressure regions were never detected in the conical tap geometry simulations (Fig. 8). Gas entrainment into a steel tap stream has been shown to significantly increase splashing at the taphole of a blast furnace and reduce the lining lifetime [3].

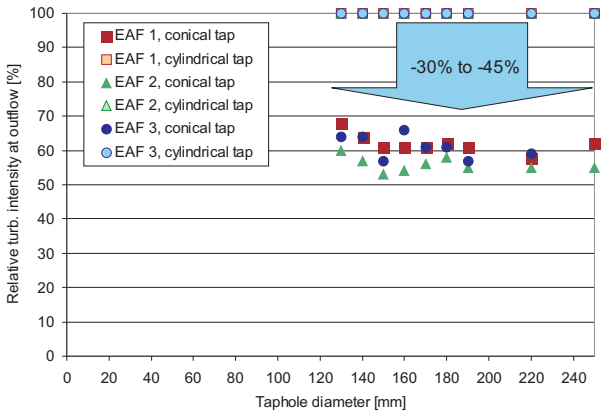

Fig. 7. Calculated mean turbulence intensities at the tap channel exit were significantly lower for the conical geometries for all tap diameters compared to the cylindrical geometries

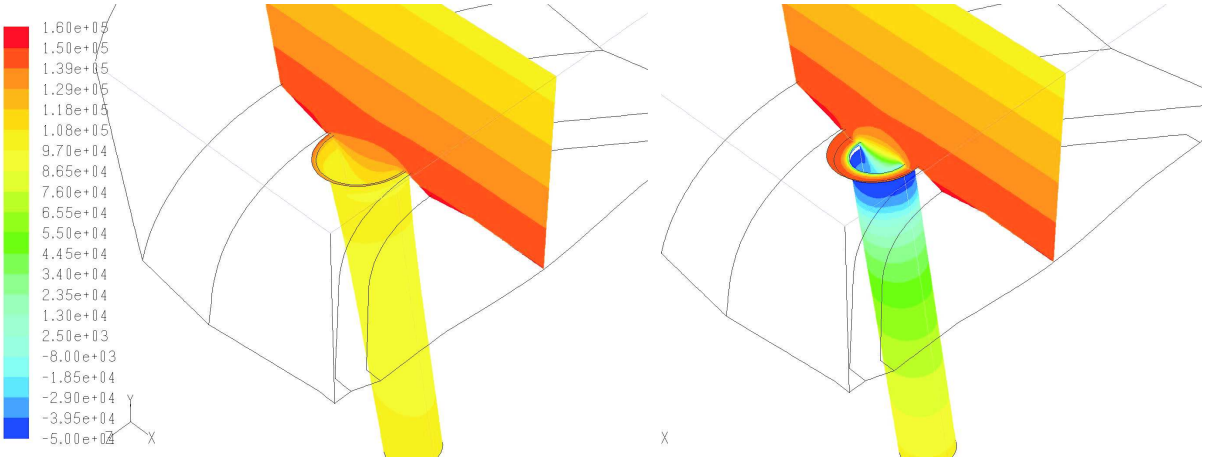

Fig. 8. Calculated static pressure $p_{stat} = p^0 + p_{ferrostat}$ in vertical cross section, at the inlet area and at the channel wall in Pa, left: conical geometry, right: conventional cylindrical geometry (EAF no. 1, 190 mm tap diameter)

3.2. Late slag entrainment

At a certain steel height above the tap inlet, the mass flow rate in the tap channel is higher than the mass flow rate to the tapping region. As a result, the surface of the steel liquid is depressed above the tapping inlet. With a higher mass flow rate in the tap channel, namely larger tap diameters at a given ferrostatic pressure at the tap exit, this depression of the steel surface occurs at an increased steel height. As a result the risk of slag entrainment into the tap channel increases with increasing mass flow rate in the tap channel, namely increasing tap diameter. From the three-dimensional CFD simulations with symmetric boundary conditions around the tap inlet, no strong indications for the formation of vortices were found with both designs.

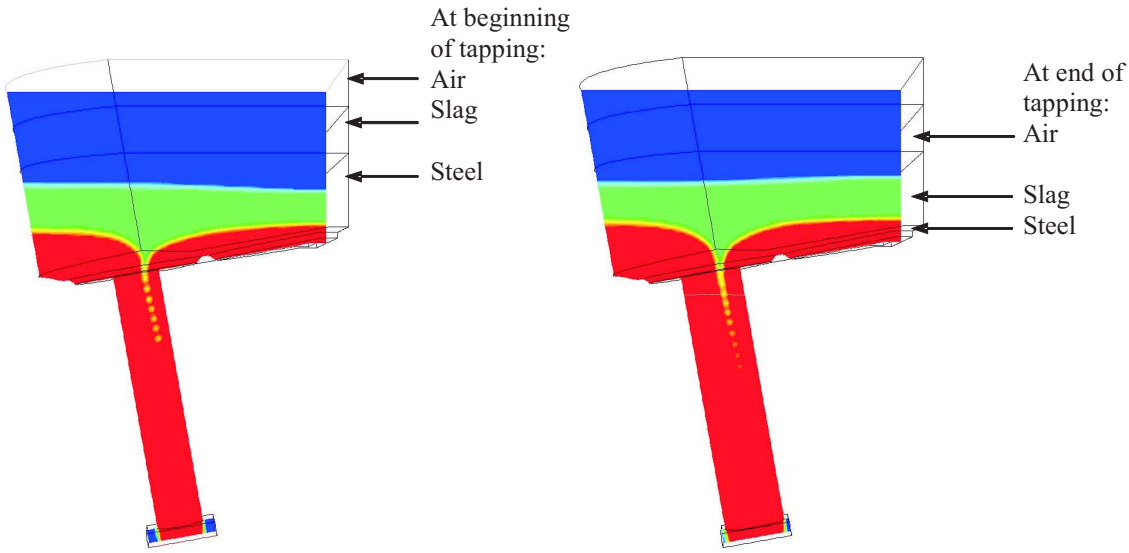

Fig. 9. Slag entrainment at the end of tapping (EAF no. 1, cylindrical design, left: 170 mm tap diameter, right: 220 mm tap diameter, vertical cross section of a three-dimensional simulation)

From the three-phase VOF simulations, the amount of remaining steel in the furnace at the time point of initial slag entrainment could be estimated (Fig. 9). With increasing tap diameter, and thereby mass flow rate, slag entrainment occurred with a larger remaining steel mass, for both tap designs. The resulting mass differences of remaining steel as a result of tapping with tap diameters between 170 mm and 220 mm ranged from 2 t (EAF no. 2) to 7 t (EAF no. 4) (i.e., 3% for EAF no. 4 and 6% for EAF no. 3) (Fig. 10). For small tap diameters slag entrainment occurred at a later stage of tapping and at lower remaining steel masses; however, the tapping time increased with decreasing tap diameter. Whilst for the two designs there was no conclusive difference between the calculated time of slag entrainment for any given diameter, in service trials are currently in progress to further evaluate this point.

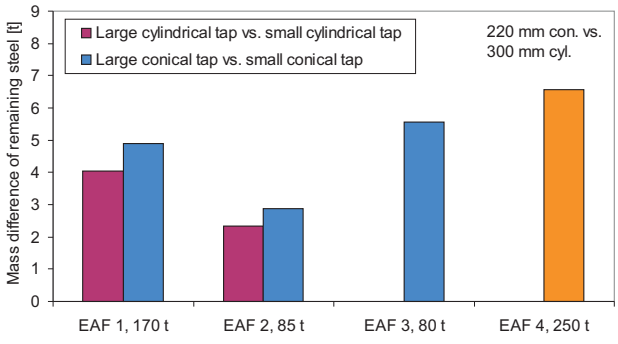

Fig. 10. Calculated difference of remaining steel mass in EAFs due to slag entrainment at the end of tapping

3.3. Decreased wear of conical bottom tapping systems

Tap channel wear depends on steel infiltration of the refractory material, the mass transport in the near-wall boundary layer, in addition to the pressure and temperature of the infiltrated zone. EAF hearth lining wear rates have been modelled as a function of static pressure (i.e., infiltration depth) and wall boundary layer thickness (i.e., mass transport) [4]. However, such a strategy does not apply to the tap channel as the channel brick open porosity is lower than that of hearth linings and static pressure at the wall layer is significantly lower due to the high steel velocity. In the fluid separation region at the cylindrical tap geometry inlet, calculated shear wall stresses in the wall boundary layer were found to be lower than for the conical design at all tap diameters. This is explained by the recirculation zone having a low steel velocity (or due to filling with gas). However, in contrast to these findings, plant experiences have shown higher erosion rates at the cylindrical tap inlet area, which results in a near conical tap geometry at the end of their lifetime.

Static pressure at the channel wall decreases from $p_{stat,max} = p^0 + p_{ferrostat}$ during melting when the tap channel is filled (with olivine sand) to $p_{stat} = p_{total} - p_{dyn} < p_{stat,max}$ during tapping. Low static pressure regions were detected in the simulations for all cylindrical geometries due to the fluid separation, but never for conical geometries (see Fig. 8).

Considering that internal self decomposition of MgO-C bricks (i.e., MgO + C = Mg + CO) occurs at CO

partial pressures near 0.01 bar (i.e., 10^3 Pa at 1600°C) it is likely that the low pressure regions of cylindrical tap systems contribute to tap brick wear. Pressures in this range were never detected in the conical design CFD simulations (see Fig. 8).

In addition to steel flow related wear, chemical corrosion may occur due to contact with slag. This is of special importance as process slags in the EAF may contain high concentrations of FeO and MnO that decrease slag viscosity and increase the MgO solubility. From phase equilibrium simulations of a highly oxidized EAF slag (i.e., 27 wt.% CaO, 10 wt.% SiO_2, 36 wt.% Fe_{tot}, 4 wt.% Al_2O_3, and 5 wt.% MnO) the MgO saturation has a calculated concentration of 5.6 wt.%. However, with the high quality magnesia lining grade used for the RHI tap channel bricks (e.g., ANKERTAP DX90) the influence of infiltrating FeO and MnO on the calculated phase equilibrium is remarkably low, due to the buffering effect of almost pure magnesia (Fig. 11). Nevertheless, whilst chemical corrosion is minimized using ANKERTAP DX90, the erosive wear mechanism due to the low viscosity of the FeO rich slag remains.

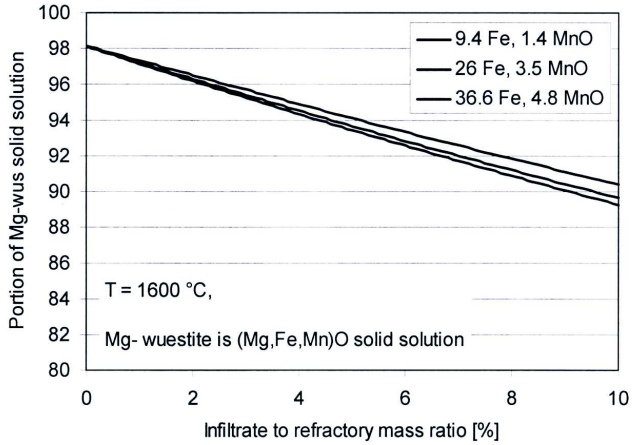

Fig. 11. Calculated percentage of Mg-wuestite in slag-infiltrated ANKERTAP DX90 at varying slag oxidation states (wt.% Fe_{tot} and MnO)

4. Conclusions–Implications for the EAF bottom tapping process

The steel flow in four EAF bottom tapping systems was investigated by CFD simulations to compare conventional cylindrical tap channel geometries with the new conical design for channel outflow diameters of between 150 mm and 300 mm. The following conclusions are apparent from the results:

- At large channel diameters (e.g., d > 250 mm) mass flow of the liquid steel approaches 2 t/s with potential deleterious effect on the steel ladle.
- In conical tapping systems, steel flow turbulence is significantly reduced by 55–70% at the tap channel outlet, compared to the cylindrical design, resulting in a more stable free jet and a lower tendency for wear.
- Very low pressure areas are avoided at the conical tap channel inlet. In contrast, fluid separation occurs at the inlet area of cylindrical tap systems. Pressures in the order of 10^3 Pa lead to internal decomposition of refractory MgO-C.
- Maximum steel flow velocities in the inlet area are significantly lower for conical tap systems when compared to cylindrical systems of same tap diameter.
- Slag entrainment occurs at a lower steel bath level with smaller tap diameters.
- The remaining steel mass in the EAF at the moment of slag entrainment is decreased for small tap diameter, resulting in a higher metal yield.

In service results have shown that the conical tap design significantly decreases inlet wear and the tap mass flow rates remain more constant during lifetime. As a result, the operating conditions are more stable over the entire tap lifetime compared to the cylindrical tap systems. In addition, the lifetime of conical tap systems is further increased by the optimized lining thickness and reduced wear at the inlet area.

Customer reports are confirming the benefits of the conical tapping system for generating a more stable free jet, decreasing tapping time, and decreasing refractory wear rate in the bottom tapping area.

REFERENCES

[1] J. Jeitler, R. Pungersek, G. Sauer, i-TAP BOF: The New Converter Taphole System. RHI Bulletin **1**, 20 (2007).

[2] J. Bachmayer, R. Sorger, Electric Arc Furnace Taphole Changing Systems. RHI Bulletin **2**, 34 (2006).

[3] Q. He, P. Zulli, F. Tanzil, J. Dunning, G. Evans, Flow Characteristics of a Blast Furnace Taphole Stream and its Effects on Trough Refractory Wear. ISIJ International **42**, 3, 235 (2002).

[4] L. F. Verdeja, R. Parra, J. P. Sancho, J. Bullon, Corrosion Mechanism and Wear Prediction of the Sole of an Electric Arc Furnace. ISIJ International **43**, 2, 192 (2003).

Received: 3 April 2008.